

**(Down-to-)Earth matter effect in supernova neutrinos**Enrico Borriello,<sup>1</sup> Sovan Chakraborty,<sup>1</sup> Alessandro Mirizzi,<sup>1</sup> Pasquale Dario Serpico,<sup>2</sup> and Irene Tamborra<sup>3</sup><sup>1</sup>*II Institut für Theoretische Physik, Universität Hamburg,  
Luruper Chaussee 149, 22761 Hamburg, Germany*<sup>2</sup>*LAPTh, Univ. de Savoie, CNRS, B.P.110, Annecy-le-Vieux F-74941, France*<sup>3</sup>*Max-Planck-Institut für Physik (Werner Heisenberg Institut), Föhringer Ring 6, 80805 München, Germany*

Neutrino oscillations in the Earth matter may introduce peculiar modulations in the supernova (SN) neutrino spectra. The detection of this effect has been proposed as diagnostic tool for the neutrino mass hierarchy at “large” 1-3 leptonic mixing angle  $\theta_{13}$ . We perform an updated study on the observability of this effect at large next-generation underground detectors (i.e., 0.4 Mton water Cherenkov, 50 kton scintillation and 100 kton liquid Argon detectors) based on neutrino fluxes from state-of-the-art SN simulations and accounting for statistical fluctuations via Monte Carlo simulations. Since the average energies predicted by recent simulations are lower than previously expected and a tendency towards the equalization of the neutrino fluxes appears during the SN cooling phase, the detection of the Earth matter effect will be more challenging than expected from previous studies. We find that none of the proposed detectors shall be able to detect the Earth modulation for the neutrino signal of a typical galactic SN at 10 kpc. It should be observable in a 100 kton liquid Argon detector for a SN at few kpc and all three detectors would clearly see the Earth signature for very close-by stars only ( $d \sim 0.2$  kpc). Finally, we show that adopting IceCube as co-detector together with a Mton water Cherenkov detector is not a viable option either.

PACS numbers: Pq, 97.60.Bw

**I. INTRODUCTION**

Physical and astrophysical diagnostics via supernova (SN) neutrino detection in underground detectors represent a subject of intense investigation in astroparticle physics. A lot of attention has been devoted to possible signatures of the Mikheyev-Smirnov-Wolfenstein (MSW) matter effect [1] on the neutrino flavor evolution in supernovae (SNe) [2]. Lately, novel phenomena have been found to be important in the region close to the neutrinosphere where the neutrino density is such that the neutrino-neutrino interactions dominate the flavor evolution. Neutrino self-interactions are responsible for large coherent conversions between different flavors (see, e.g., [3] for a recent review). Neutrino oscillations in SNe could imprint peculiar signatures on the observable neutrino signal, sensitive to the neutrino mass and mixing, and to the unknown mass hierarchy [4].

Due to the uncertainties in the calculation of the primary SN neutrino spectra, it seems difficult to establish oscillation effects solely on the basis of theoretical expectations. Therefore the importance of relatively model-independent signatures has been emphasized in the recent literature, e.g. in association with the prompt  $\nu_e$  neutronization burst [5], with the rise time of the early neutrino signal [6], or with matter effects associated to the shock-wave propagation at late times [7–11]. One unequivocal signature would be the observation of the Earth matter effects [2, 12, 13]. They induce a characteristic energy-dependent modulation on the measured flux when SN neutrinos cross the Earth matter before being detected. Earth matter effects could be measured in a single detector, if it has enough energy resolution and statistics to track the wiggles in the observed energy spectrum. A Fourier analysis of the SN neutrino signal has been proposed as a powerful tool to diagnose this modulation [14, 15]. Moreover, the comparison of the signals from shadowed and unshadowed detectors may allow one to diagnose the Earth effects even if a single detector could not resolve the modulations [16].

Recent supernova simulations indicate lower average energies than previously expected [6, 17, 18] and a tendency towards the equalization of the neutrino fluxes during the cooling phase, i.e. for post-bounce times  $t \gtrsim 1$  s [18, 19]. Remarkably, this trend eases the agreement of theoretical expectations with SN 1987A data [20, 21]. Motivated by this new input and since the observability of the Earth matter effect largely depends on the neutrino average energies and on the flavor-dependent differences among the primary spectra, we find worthwhile to reevaluate the detectability of the Earth matter effects in large detectors. We refer to three classes of detectors proposed for low-energy neutrino physics and astrophysics, viz. water Cherenkov (WC) detectors with fiducial masses of  $\mathcal{O}(400)$  kton [22, 23], liquid scintillation (SC) detectors with masses of  $\mathcal{O}(50)$  kton [24], and Liquid Argon Time Projection Chambers (LAr TPC) with fiducial masses of  $\mathcal{O}(100)$  kton [25]. These three detection techniques are the backbones of the European project LAGUNA (Large Apparati for Grand Unification and Neutrino Astrophysics) [26] and the LBNE (Long Baseline Neutrino Experiment) towards DUSEL (Deep Underground Science and Technology Laboratory) in the US [27]. Moreover, the project of the Mton-class WC detector Hyper-Kamiokande is currently discussed in Japan [23]. In particular, WC and SC neutrino experiments are mostly sensitive to SN  $\bar{\nu}_e$  through the inverse beta decay process

$\bar{\nu}_e + p \rightarrow n + e^+$ . On the other hand, LAr TPC would have a high sensitivity to SN  $\nu_e$ 's, through the charged current interactions of  $\nu_e$  with the Ar nuclei in the detector. We also consider the Icecube ice Cherenkov detector [28] as “co-detector” to monitor the Earth effect in comparison with the energy-integrated signal measured in a Mton WC detector [16].

For all these detectors, we find that no signature of the Earth matter effect is observable for a typical galactic SN at  $d \simeq 10$  kpc. In the more optimistic case of a close-by SN at  $d = 1$  kpc, the chances to detect the Earth matter signature appear statistically weak in the antineutrino signal. Conversely, a signal would show up in the  $\nu_e$  signal detectable at a LAr TPC. The Earth matter signal would be detectable with high significance in both neutrino and antineutrino signals for relatively close by stars which might evolve into core-collapse SNe at unpredictable future times, like Betelgeuse, Mira Ceti and Antares (at  $d \lesssim 0.2$  kpc) — provided that the electronics of the detector will be able to cope with such a huge rate of events. Our results allow us to conclude that the previous paradigm on the observability of the SN neutrino Earth matter effects was based on an “optimistic” choice of the non-oscillated neutrino fluxes, not anymore confirmed by the most recent and less approximated SN simulations.

The plan of our work is as follow. In Sec. II we present the neutrino signal from SN hydrodynamical simulations we adopt as benchmark for our study. In Sec. III we characterize the SN neutrino flavor conversions and the Earth matter effect. In Sec. IV the features of our reference detectors (fiducial mass, cross sections and energy resolution) are described. In Sec. V our results on the detectability of the Earth effect in each of the reference detectors are presented. Comments and conclusions are illustrated in Sec. VI.

## II. NUMERICAL MODELS FOR SUPERNOVA NEUTRINO EMISSION

The un-oscillated  $\nu$  distributions (with  $\nu = \{\nu_e, \bar{\nu}_e, \nu_x (= \nu_\mu, \nu_\tau)\}$ ) are parametrized in energy and time as follows

$$F_\nu^0(E, t) = \phi_\nu(t) f_\nu(E, t) = \frac{L_\nu(t)}{\langle E_\nu(t) \rangle} f_\nu(E, t) , \quad (1)$$

where  $\phi_\nu(t)$  is the *energy-integrated* neutrino number flux for each post-bounce time  $t$ ,  $L_\nu(t)$  the luminosity and  $\langle E_\nu(t) \rangle$  the mean neutrino energy. The function  $f_\nu(E, t)$  is the energy spectrum, normalized such that  $\int dE f_\nu(E, t) = 1$ . It is parametrized as in [29]

$$f_\nu(E, t) = \frac{1}{\langle E_\nu(t) \rangle} \frac{(1 + \alpha_\nu(t))^{1 + \alpha_\nu(t)}}{\Gamma(1 + \alpha_\nu(t))} \left( \frac{E}{\langle E_\nu(t) \rangle} \right)^{\alpha_\nu(t)} \exp \left[ -(1 + \alpha_\nu(t)) \frac{E}{\langle E_\nu(t) \rangle} \right] , \quad (2)$$

where the energy-shape parameter  $\alpha_\nu(t)$  is [29, 30]

$$\alpha_\nu(t) = \frac{2\langle E_\nu(t) \rangle^2 - \langle E_\nu(t)^2 \rangle}{\langle E_\nu(t)^2 \rangle - \langle E_\nu(t) \rangle^2} . \quad (3)$$

The variables  $L_\nu(t)$ ,  $\langle E_\nu(t) \rangle$  and  $\alpha_\nu(t)$  are extracted from SN simulations.

In the following we adopt as input the recent SN simulations performed by the Garching group (G) —see [6] for references— and by the Basel/Darmstadt group (B/D) [17]. In Fig. 1 we show the initial luminosities  $L_\nu$  (upper panels), average energies  $\langle E_\nu \rangle$  (middle panels) and time-integrated energy-spectra in different time windows (lower panels) for the different flavors  $\nu_e$ ,  $\bar{\nu}_e$  and  $\nu_x$  and for the simulations from the two groups: i) accretion phase of a  $15 M_\odot$  progenitor from the Garching group (left panel); ii) accretion and cooling phases of a  $18 M_\odot$  progenitor from the Basel/Darmstadt group (middle panels for the accretion and right panels for the cooling).

In the former case, the accretion phase is clearly visible in the neutrino light-curve. It lasts till  $t \simeq 0.2$  s and appears as a pronounced hump in the electron (anti)neutrino luminosities. The relative time-integrated spectra for the accretion phase (with  $t \in [0, 0.25]$  s) show that flavor-dependent flux differences are large, with a robust hierarchy for the time-integrated neutrino number fluxes ( $\Phi_\nu^0 = \int dt \phi_\nu(t)$ ), namely  $\Phi_{\nu_e}^0 > \Phi_{\bar{\nu}_e}^0 \gg \Phi_{\nu_x}^0$ . Therefore, the accretion phase would represent the best time-window to detect effects of flavor conversions.

The Basel/Darmstadt simulations have an accretion phase lasting till  $t \simeq 0.4$  s (middle panel). The main features of the neutrino signal are similar to the ones of the Garching case. These simulations provide the late-time SN neutrino signal from the cooling phase too, shown in the right panels of Fig. 1. During the cooling phase all neutrino flavors originate close to the neutron star surface, where the material is neutron rich, suppressing charged-current reactions for  $\bar{\nu}_e$ . Therefore, the luminosities and the average energies of  $\bar{\nu}_e$  and  $\bar{\nu}_x$  become quite similar. As a result, the time-integrated neutrino fluxes in  $t \in [1.0, 10.0]$  s are so close that one expects to be difficult to measure oscillation effects in this case.

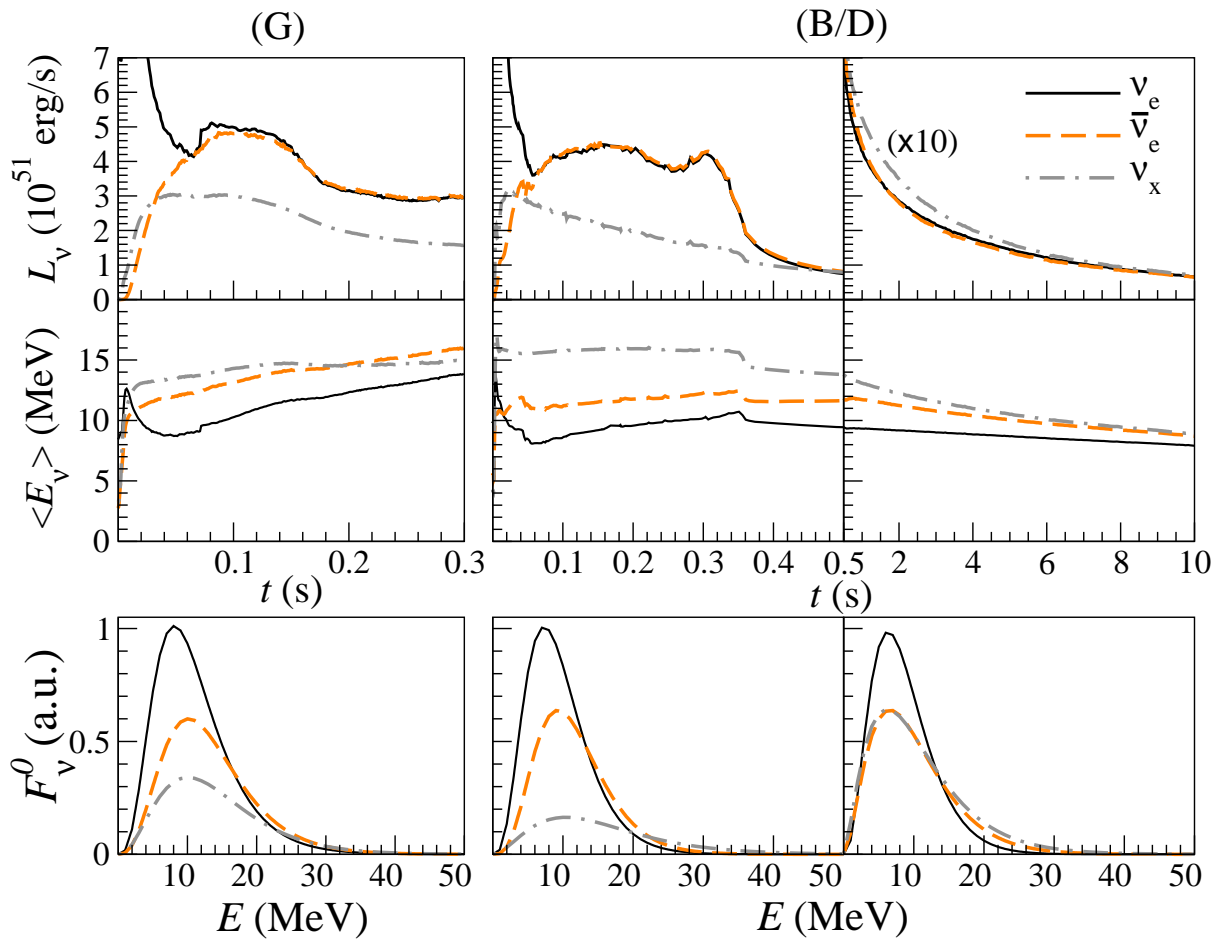


FIG. 1: Time evolution of neutrino luminosities  $L_\nu$  (upper panels), average energies  $\langle E_\nu \rangle$  (middle panels) and time-integrated energy spectra (lower panels) for  $\nu_e$  (continuous curve),  $\bar{\nu}_e$  (dashed curve), and  $\nu_x$  (dash-dotted curve). The left panels refer to the accretion phase of a Garching simulation for a  $15.0 M_\odot$  progenitor, while the other ones to a Basel/Darmstadt simulation for a  $18.0 M_\odot$  for the accretion (central panels) and cooling (right panels) phase.

In Table I we report the parameters of the time-integrated SN neutrino spectra for the Garching and the Basel/Darmstadt simulations distinguishing between the accretion ( $t \leq 0.25$  s for G and  $t \leq 0.4$  s for B/D) and the cooling phase. These parameters will be taken as benchmark for the evaluation of the Earth matter effect. From this Table, it is evident that the neutrino average energies provided by the recent SN simulations are significantly lower than what assumed in the previous studies (see, e.g. Table 3 of [14]).

### III. FLAVOR CONVERSIONS AND EARTH MATTER EFFECT

#### A. Neutrino mixing parameters

We assume the three neutrino mass eigenstates separated by the following neutrino mass squared differences as from the global  $3\nu$  oscillation analysis [31]

$$\Delta m_{\text{atm}}^2 = m_3^2 - m_{1,2}^2 = 2.35 \times 10^{-3} \text{ eV}^2, \quad (4)$$

$$\Delta m_{\odot}^2 = m_2^2 - m_1^2 = 7.54 \times 10^{-5} \text{ eV}^2. \quad (5)$$

Since the sign of  $\Delta m_{\text{atm}}^2$  is not determined yet, we will consider both normal (NH,  $\Delta m_{\text{atm}}^2 > 0$ ) and inverted hierarchy (IH,  $\Delta m_{\text{atm}}^2 < 0$ ) scenarios. The mass eigenstates are related to the flavor eigenstates ( $\nu_e, \nu_\mu, \nu_\tau$ ) by means of three

TABLE I: Spectral-fit parameters for the neutrino and antineutrino fluxes integrated over the accretion phase of the  $15 M_{\odot}$  Garching progenitor (G) and both the accretion and cooling phases of the  $18 M_{\odot}$  Basel/Darmstadt (B/D) progenitor.

Model	$\langle E_{\nu_e} \rangle$ (MeV)	$\langle E_{\nu_x} \rangle$ (MeV)	$\Phi_{\nu_e}^0 (\times 10^{56})$	$\Phi_{\nu_x}^0 (\times 10^{56})$	$\alpha_{\nu_e}$	$\alpha_{\nu_x}$
G (accretion, $t \leq 0.25$ s)	10.9	14.0	5.68	2.67	3.1	2.5
B/D (accretion, $t \leq 0.4$ s)	9.5	15.6	8.53	3.13	3.4	2.0
B/D (cooling, $t > 1.0$ s)	8.6	10.5	11.80	10.75	2.8	1.5

Model	$\langle E_{\bar{\nu}_e} \rangle$ (MeV)	$\langle E_{\bar{\nu}_x} \rangle$ (MeV)	$\Phi_{\bar{\nu}_e}^0 (\times 10^{56})$	$\Phi_{\bar{\nu}_x}^0 (\times 10^{56})$	$\alpha_{\bar{\nu}_e}$	$\alpha_{\bar{\nu}_x}$
G (accretion, $t \leq 0.25$ s)	13.2	14.0	4.11	2.67	3.3	2.5
B/D (accretion, $t \leq 0.4$ s)	11.6	15.6	7.51	3.13	4.0	2.0
B/D (cooling, $t > 1.0$ s)	10.0	10.5	9.74	10.75	1.9	1.5

mixing angles. Their best-fit values, as in the global  $3 \nu$  oscillation analysis in [31], are

$$\sin^2 \theta_{13} = 0.02 \quad \text{and} \quad \sin^2 \theta_{12} = 0.31 . \quad (6)$$

The mixing angle  $\theta_{23}$  is not relevant for our purposes since we are assuming equal  $\nu_{\mu}$  and  $\nu_{\tau}$  fluxes.

### B. No Earth crossing

The emitted SN neutrino flux is processed by self-induced and MSW oscillation effects during its propagation. The self-induced effects would take place within  $r \sim \mathcal{O}(10^3)$  km from the neutrinosphere whereas the MSW transitions take place at larger radii, in the region  $r \sim 10^4$ – $10^5$  km. As the self-induced and MSW effects are widely separated in space, they can be considered independently of each other.

We start considering the accretion phase. No self-induced flavor conversion occurs in NH and for the spectral ordering of the accretion phase [32–34]. Instead, potentially large self-induced effects could be expected for neutrinos and antineutrinos in IH [32–34]. However, it has been shown using results both from Basel/Darmstadt group simulations and Garching group ones [35–39] that the multi-angle effects associated with the dense ordinary matter suppress collective oscillations in iron-core SNe [40].

The neutrino fluxes can only undergo the traditional MSW conversions in SNe while passing through the outer layers of the star. Therefore, it is straightforward to compute the  $\bar{\nu}_e$  flux at the Earth in the different cases [2]. Recently reactor experiments measured “large”  $\theta_{13}$  [41, 42], for such value of the mixing angle and in NH, one finds

$$F_{\bar{\nu}_e} = \cos^2 \theta_{12} F_{\bar{\nu}_e}^0 + \sin^2 \theta_{12} F_{\bar{\nu}_x}^0 \quad \text{and} \quad F_{\nu_e} = F_{\nu_x}^0 . \quad (7)$$

Instead, in IH one gets

$$F_{\bar{\nu}_e} = F_{\bar{\nu}_x}^0 \quad \text{and} \quad F_{\nu_e} = \sin^2 \theta_{12} F_{\nu_e}^0 + \cos^2 \theta_{12} F_{\nu_x}^0 . \quad (8)$$

Concerning the cooling phase, the characterization of the flavor conversions is less straightforward. Indeed, it is expected that self-induced flavor oscillations would be no longer inhibited by the ordinary matter density and multiple spectral splits should occur [43, 44]. However, since the spectral differences among different flavors are not large (see Fig. 1), we numerically checked that the effect of the self-induced oscillations would produce a flavor equilibration among the different neutrino species (see also [34, 45]). This would reduce the possibility to observe any signature of Earth matter effects. Moreover, it is expected that at  $t \gtrsim 2$  s the non-adiabatic effects associated with the matter turbulences in the supernova envelope would produce a smearing of the MSW flavor conversions [10, 46, 47] further reducing the spectral differences. In the following, we will neglect all these complicated effects and we will assume that the oscillated fluxes are described by Eqs. (7)–(8) during the cooling phase too, since we are interested in the time-integrated signal. Our approach is conservative, since the experimental detectability of the Earth matter signature would be even more challenging than in our simplified scenario.

### C. Earth crossing

If the supernova is shadowed by the Earth for a detector [48], neutrinos will travel a certain distance through the Earth and therefore will undergo Earth matter oscillations during their propagation. Since neutrinos arrive at

the Earth as mass eigenstates, the net effect of oscillations can be written in terms of the conversion probabilities  $P_{i\bar{e}} = P(\nu_i \rightarrow \nu_e)$ . For large  $\theta_{13}$ , the neutrino fluxes at the Earth are [2]

$$F_{\nu_e}^{\oplus} = (1 - P_{2e})F_{\nu_e}^0 + P_{2e}F_{\nu_x}^0 \quad (9)$$

and for antineutrinos

$$F_{\bar{\nu}_e}^{\oplus} = (1 - \bar{P}_{2e})F_{\bar{\nu}_e}^0 + \bar{P}_{2e}F_{\bar{\nu}_x}^0 \quad (10)$$

Here  $P_{2e} \equiv P(\nu_2 \rightarrow \nu_e)$  and  $\bar{P}_{2e} \equiv P(\bar{\nu}_2 \rightarrow \bar{\nu}_e)$  while propagating through the Earth. The analytical expressions for  $P_{2e}$  and  $\bar{P}_{2e}$  can be calculated for the approximate two-density model of the Earth [15]. When neutrinos traverse a distance  $L$  through the mantle of the Earth, these quantities assume a very simple form [2, 12]:

$$P_{2e} = \sin^2 \theta_{12} + \sin 2\theta_{12}^m \sin(2\theta_{12}^m - 2\theta_{12}) \sin^2 \left( \frac{\Delta m_{\odot}^2 \sin 2\theta_{12}}{4E \sin 2\theta_{12}^m} L \right), \quad (11)$$

$$\bar{P}_{2e} = \sin^2 \theta_{12} + \sin 2\bar{\theta}_{12}^m \sin(2\bar{\theta}_{12}^m - 2\theta_{12}) \sin^2 \left( \frac{\Delta m_{\odot}^2 \sin 2\theta_{12}}{4E \sin 2\bar{\theta}_{12}^m} L \right), \quad (12)$$

where  $\theta_{12}^m$  and  $\bar{\theta}_{12}^m$  are the effective values of  $\theta_{12}$  in the Earth matter for neutrinos and antineutrinos, respectively [49]. The Earth crossing induces a peculiar oscillatory signature in the energy spectra and from Eqs. (7)–(10), one would expect the Earth matter effect for antineutrinos in NH and for neutrinos in IH.

#### D. Power spectrum of the Earth matter signal

The typical event rate associated with an inverse beta decay process is  $\propto E^2 F_{\bar{\nu}_e}^{\oplus}(E)$ , the cross section being  $\sigma \propto E^2$ . Whereas the distance between the energy-spectrum peaks due to the Earth modulation increases with energy, the peaks are nearly equally spaced in the inverse energy spectrum. In order to show this behavior, it is useful to recast the  $\nu_e$  and  $\bar{\nu}_e$  fluxes as [14]

$$F_{\nu_e}^{\oplus} = \sin^2 \theta_{12} F_{\nu_e}^0 + \cos^2 \theta_{12} F_{\nu_x}^0 + \Delta F^0 A_{\oplus} \sin^2 \left( \frac{\overline{\Delta m_{\odot, \nu}^2}}{10^{-5} \text{ eV}^2} \frac{L}{10^3 \text{ km}} y \right), \quad (13)$$

$$F_{\bar{\nu}_e}^{\oplus} = \cos^2 \theta_{12} F_{\bar{\nu}_e}^0 + \sin^2 \theta_{12} F_{\bar{\nu}_x}^0 - \Delta \bar{F}^0 \bar{A}_{\oplus} \sin^2 \left( \frac{\overline{\Delta m_{\odot, \bar{\nu}}^2}}{10^{-5} \text{ eV}^2} \frac{L}{10^3 \text{ km}} y \right), \quad (14)$$

where  $\Delta F^0 = F_{\nu_e}^0 - F_{\nu_x}^0$  is the energy-dependent difference of the primary neutrino spectra and  $A_{\oplus} = \sin(2\theta_{12}^m - 2\theta_{12})$ ; we also defined the mass squared difference in the Earth  $\overline{\Delta m_{\odot, \nu}^2} = \Delta m_{\odot}^2 \sin 2\theta_{12} / \sin 2\theta_{12}^m$  and the ‘‘inverse energy variable’’  $y = 12.5 \text{ MeV}/E$ . Analogous definitions hold in the antineutrino sector in terms of the difference of the antineutrino spectra and of  $\bar{\theta}_{12}^m$ . The Earth matter effects on SN neutrino signal can thus be identified at a single detector through peaks in the Fourier transform of the inverse energy spectrum [14]. The neutrino signal is observed as a discrete set of events. Following [14], we define the power spectrum of the  $N$  detected events as

$$G_N(k) \equiv \frac{1}{N} \left| \sum_{i=1}^N e^{iky_i} \right|^2. \quad (15)$$

This function is related to the continuous power spectrum,  $G(k)$ , by means of the function  $q(y) \propto E^2 F_{\bar{\nu}_e}^{\oplus}(E)$ :

$$G_N(k) = N \left| \frac{1}{N} \sum_{i=1}^N e^{iky_i} \right|^2 = N \left| \langle e^{iky} \rangle \right|^2 \approx N \left| \int dy q(y) e^{iky} \right|^2 \equiv N G(k). \quad (16)$$

Figure 2 shows the power spectrum  $G(k)$  of the function  $q(y)$  as a function of  $k$ , for an illustrative purpose. Note that the Earth effects introduce peaks in the power spectrum at specific frequencies. In particular, we aim at discussing the dependence of  $G(k)$  on the ratio of the initial fluxes  $\Phi_{\bar{\nu}_e}^0 / \Phi_{\bar{\nu}_x}^0$  (left panels), and on the difference among the neutrino average energies  $\langle E_{\bar{\nu}_x} \rangle - \langle E_{\bar{\nu}_e} \rangle$  (right panels). We take as benchmark values the ones used in [14], that refer to previous Garching simulations [50] and we fix  $\langle E_{\bar{\nu}_e} \rangle = 15 \text{ MeV}$  and  $\alpha_{\bar{\nu}_e} = \alpha_{\bar{\nu}_x} = 3.0$ . In the left panel, we assume  $\langle E_{\bar{\nu}_x} \rangle = 18 \text{ MeV}$  and vary the ratio of the total fluxes  $\Phi_{\bar{\nu}_e}^0 / \Phi_{\bar{\nu}_x}^0$  between 0.8 and 1.5. The two extreme cases are

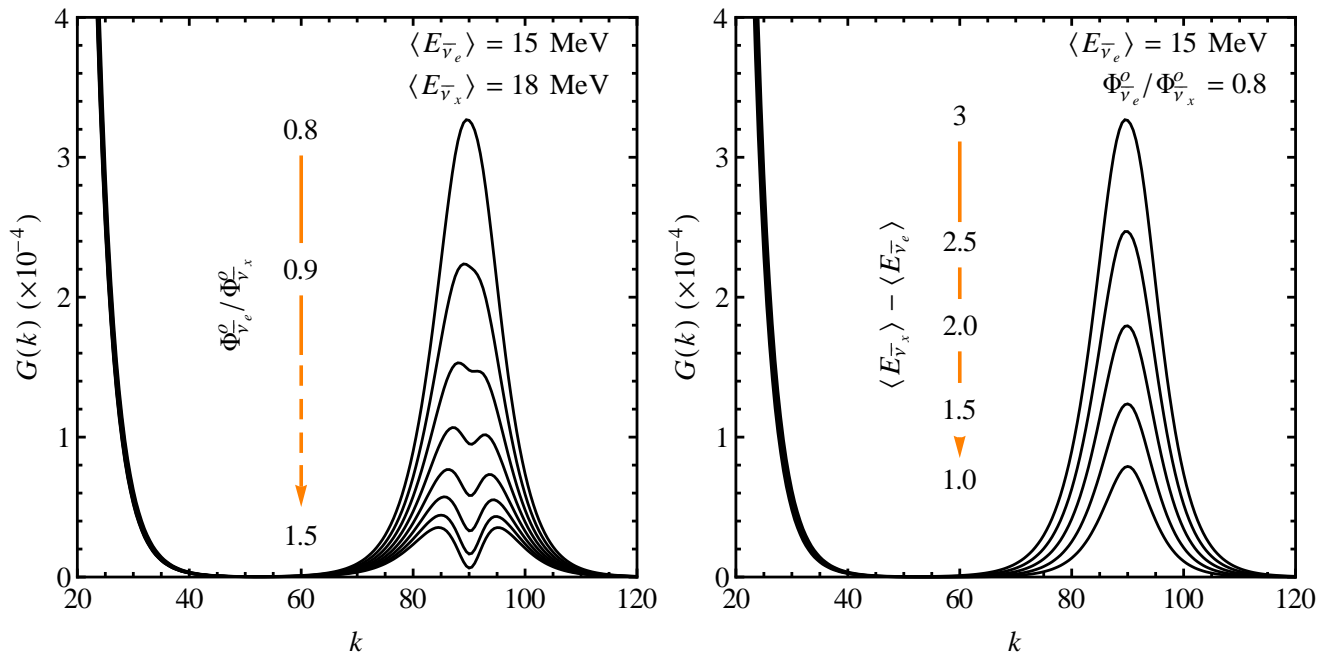


FIG. 2: Power spectrum  $G(k)$  of the Earth matter signal. The left panel shows  $G(k)$  for a flux ratio varying in the range  $0.8 < \Phi_{\bar{\nu}_e}^0/\Phi_{\bar{\nu}_x}^0 < 1.5$ , while the right panel shows the impact of the change of the difference of the average energies in the range  $1 \text{ MeV} < \langle E_{\bar{\nu}_x} \rangle - \langle E_{\bar{\nu}_e} \rangle < 3 \text{ MeV}$ .

representative of the flux ordering during the cooling and the accretion phase, respectively. The large peak in  $G(k)$  at low values of  $k$  is the dominant contribution due to the first two terms in Eq. (14). The peak at  $k \simeq 90$  corresponds to the oscillations in the Earth matter. Since  $\bar{\nu}_e$ 's have lower average energy than  $\bar{\nu}_x$ 's, and due to the suppression at low-energy associated with the  $E^2$  dependence in the cross section, the peak decreases significantly increasing the ratio  $\Phi_{\bar{\nu}_e}^0/\Phi_{\bar{\nu}_x}^0$ . In the right panel, instead, we fix  $\Phi_{\bar{\nu}_e}^0/\Phi_{\bar{\nu}_x}^0 = 0.8$  and vary  $\langle E_{\bar{\nu}_x} \rangle$  between 15 and 18 MeV. As expected, since reducing the difference among the average energies,  $E^2 \Delta \bar{F}^0$  becomes smaller, the peak in the power spectrum is strongly suppressed.

From this parametric study, we expect that the detection of the Earth peak would be more challenging than what reported in the previous literature for the SN models described in Sec. II. In fact the trend shown in Fig. 2 is also illustrative of the expected differences in the power spectrum adopting old and more recent supernova simulation inputs. The average energies that we adopt for different  $\nu$  species are lower and closer among themselves than previously assumed. Therefore, we expect that the recent data, both for the accretion and the cooling phase, would produce a power spectrum with a significant suppression of the expected peak, similar to the one with the smallest difference  $\langle E_{\bar{\nu}_x} \rangle - \langle E_{\bar{\nu}_e} \rangle$  (see right panel of Fig. 2). We will present a quantitative estimation of this effect in the following Sections.

We now comment on the appearance of the double-peak feature as the ratio  $\Phi_{\bar{\nu}_e}^0/\Phi_{\bar{\nu}_x}^0$  decreases shown in the left panel of Fig. 2. This is another feature depending on the adopted fluxes that was not previously found in the literature. Figure 3 refers to the uppermost and lowermost curves of the left panel of Fig. 2. We assume them as representative cases of a single-peaked (upper right panels) or a double-peaked (lower right panels) power spectrum, respectively. The left panels of Fig. 3 show the contributions of  $\bar{\nu}_e$  and  $\bar{\nu}_x$  to the observable signal  $E^2 F_{\bar{\nu}_e}^\oplus$  while the right panels show the different contributions to the power spectrum. It is worthwhile to notice that the power-spectrum  $G(k)$  of the signal [Eq. (16)] can be decomposed as

$$G(k) = G_{\bar{\nu}_e}(k) + G_{\bar{\nu}_x}(k) + G_{\bar{\nu}_e \bar{\nu}_x}(k), \quad (17)$$

where the first contribution on the right-hand-side is associated with  $E^2(1 - \bar{P}_{2e})F_{\bar{\nu}_e}^0$ , the second with  $E^2\bar{P}_{2e}F_{\bar{\nu}_x}^0$ , and the third with the cross-correlation of the previous two. The three terms in the power-spectrum are peaked at very similar frequencies. Since  $G_{\bar{\nu}_e \bar{\nu}_x}(k)$  can assume negative values, it can sometimes determine the appearance of the double-peak feature, especially when the positive and negative terms become comparable, as in the lower right panel of Fig. 3.

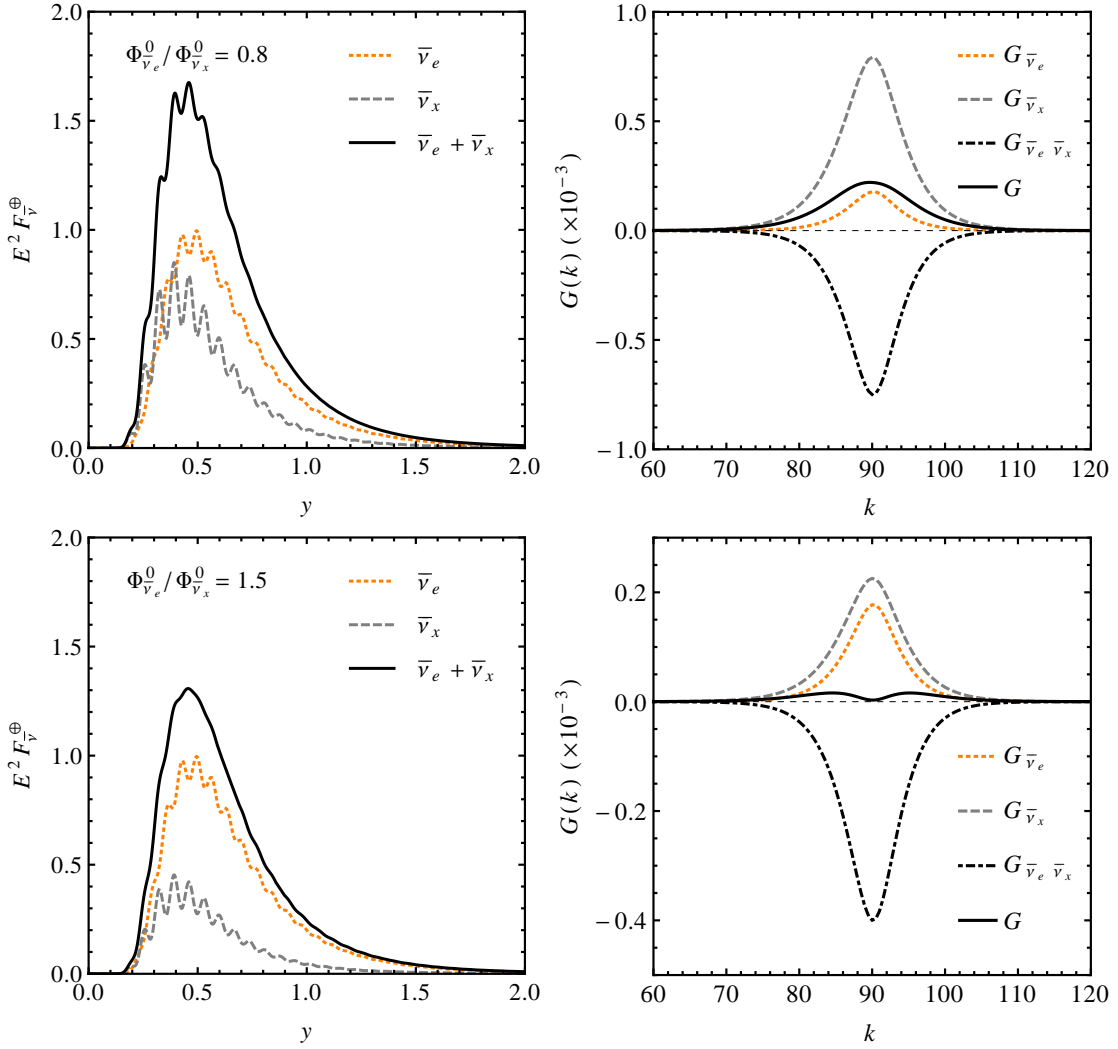


FIG. 3: Left panels: Contributions of the different flavors to the observable Earth-modulated signal  $E^2 F_y^\oplus$ , corresponding to the uppermost and lowermost cases of left panel in Fig. 2. The continuous curve represents the total  $E^2 F_y^\oplus$  flux, the short-dashed one corresponds to  $E^2(1 - \bar{P}_{2e})F_{\bar{\nu}_e}^0$ , while the long-dashed one to  $E^2 \bar{P}_{2e} F_{\bar{\nu}_x}^0$  (see Eq. 14). Right panels: Contributions to the power-spectrum  $G(k)$  as from Eq. 17. The continuous curve represents the total power-spectrum  $G(k)$ , the short-dashed one corresponds to  $G_{\bar{\nu}_e}(k)$ , the long-dashed one corresponds to  $G_{\bar{\nu}_x}(k)$ , while the dashed-dotted curve is for  $G_{\bar{\nu}_e \bar{\nu}_x}(k)$  (see text for details).

#### IV. NEUTRINO DETECTION

In this Section we describe the main aspects and ingredients of our calculations of supernova neutrino event rates. The oscillated SN neutrino fluxes at the Earth,  $F_\nu$ , must be convolved with the differential cross section  $\sigma_e$  for electron or positron production, as well as with the energy resolution function  $R_e$  of the detector, and the efficiency  $\varepsilon$  (that we assume equal to one above the energy threshold), in order to finally get observable event rates [51]:

$$N_e = F_\nu \otimes \sigma_e \otimes R_e \otimes \varepsilon. \quad (18)$$

We will now describe the main characteristics of four types of detectors we have used to calculate the signals in the presence of the Earth matter effects, namely water Cherenkov detectors, scintillation detectors, liquid Argon Time Projection Chambers, and ice Cherenkov detector Icecube.

### A. Water Cherenkov detectors

In large WC detectors, the dominant channel for supernova neutrino detection is the inverse beta decay of electron antineutrinos<sup>1</sup>

$$\bar{\nu}_e + p \rightarrow n + e^+ . \quad (19)$$

For this process, we take the differential cross section from [52]. The total cross section grows approximatively as  $E^2$ . We fold the differential cross sections for  $e^+$  production with a Gaussian energy resolution function of width  $\Delta$ . The value of  $\Delta$  is predominantly determined by the photocathode coverage of the detector. For our calculations we assume [51]

$$\Delta_{\text{WC}}/\text{MeV} = 0.47\sqrt{E_e/\text{MeV}} , \quad (20)$$

where  $E_e$  is the true positron energy. We assume as fiducial volume 400 kton [26].

### B. Scintillation detectors

In liquid SC detectors, the main channel for SN neutrino detection is the inverse beta decay of  $\bar{\nu}_e$ 's, the same as that in WC. However, here the positrons are detected through photons produced in the scintillation material. Since a larger number of photons can be produced in a SC detector, these have typically a much better energy resolution than the WC detectors. The energy resolution of the SC detectors is determined by the number of photo-electrons produced per MeV, which for this type of detectors is expected to be given by as good as [53]

$$\Delta_{\text{SC}}/\text{MeV} = 0.07\sqrt{E_e/\text{MeV}} . \quad (21)$$

Indeed, the energy resolution of a SC detector may be better by more than a factor of 6 than a WC. Since the Earth matter oscillations described in the previous section may get smeared out by the finite energy resolution of the detector, it is clear that the energy resolution plays a crucial role in the efficiency of detecting Earth effects. For our studies, we assume a fiducial mass of 50 kton [24].

### C. Liquid Argon Time Projection Chambers

LAr TPC detectors would be particularly sensitive to SN electron neutrinos through their charged current interactions with Ar nuclei

$$\nu_e + {}^{40}\text{Ar} \rightarrow {}^{40}\text{K}^* + e^- , \quad (22)$$

which proceed via the creation of an excited state of  ${}^{40}\text{K}$  and its subsequent gamma decay. The Q-value for this inverse beta decay process is 1.505 MeV. The cross-section for the charged current reaction is taken from [54]. The one for leptons in LAr TPC has been calculated by the ICARUS collaboration which reports [55]

$$\Delta_{\text{LAr}}/\text{MeV} = 0.11\sqrt{E_e/\text{MeV}} + 0.02 E_e/\text{MeV} . \quad (23)$$

The fiducial volume for SN neutrino detection is taken to be 100 kton [56].

### D. Icecube

A galactic SN  $\nu$  burst would be detectable in Icecube by a sudden, correlated increase in the photomultiplier count rate on a timescale on the order of 10 s (see Ref. [57] for a recent description). In its complete configuration and with its data acquisition system, IceCube has 5160 optical modules [57] and about 3 Mton effective detection volume,

---

<sup>1</sup> We will neglect the subleading neutrino interaction channels in the detectors, assuming that they can be separated at least on a statistical basis.



representing the largest current detectors for SN neutrinos. The SN neutrinos streaming through the antarctic ice interact mostly through  $\bar{\nu}_e + p \rightarrow n + e^+$  reactions. While fine-grained detectors, like WC detectors, reconstruct individual neutrinos on an event-by-event basis, IceCube only picks up the average Cherenkov glow of the ice. The detection rate is given by [6, 16]

$$\mathcal{R}_{\bar{\nu}_e} = \int_0^\infty dE F_{\bar{\nu}_e} E_{\text{rel}}(E) \sigma(E), \quad (24)$$

with  $E_{\text{rel}}(E)$  being the energy released by a neutrino of energy  $E$  and  $\sigma(E)$  the inverse beta-decay cross section. All other detector parameters (angular acceptance range, average quantum efficiency, number of useful Cherenkov photons per deposited neutrino energy unit, average lifetime of Cherenkov photons, effective photo cathode detection area) have been fixed to the fiducial values adopted in [16], to which we address to for further details.

## V. DETECTING EARTH MATTER EFFECT

### A. Single detector

We present our results about the detectability of the Earth effect. For our numerical calculations, we assume the mass-mixing parameters as in Eqs. (4–6). Note that, although we stick to the best fit values of the most recent  $3\nu$  global analysis, our conclusions do not qualitatively change for small variations of the adopted numerical values of the mixing parameters. We will also assume that the path-length crossed by neutrinos in the Earth is  $L = 6000$  km.

Figure 4 shows the power-spectrum  $G_N(k)$  [defined as in Eq. (15)] of the SN  $\nu$  signal in the WC (upper panels), SC (central panels) and LAr TPC detectors (lower panels). We discuss the results for three different SN distances from Earth ( $d = 10, 1, 0.2$  kpc). Since the Earth matter probability is time-independent, we consider as neutrino signal the time-integrated rate during the accretion phase taken from the  $15 M_\odot$  Garching SN simulation (see Sec. 2 and Table I for the time-integrated flux parameters). We produce 10, 50 or 100 realizations of the SN neutrino spectra at the Earth via Montecarlo simulations. The thin gray lines in Fig. 4 correspond to different realizations of  $G_N(k)$  [Eq. (15)]. The thick black line corresponds to the power-spectrum averaged over the different realizations  $G_N(k)$ . The light band around the average corresponds to the  $\pm 1\sigma$  level.

As it was already pointed out in [14], the frequency range at which the peak (or peaks) of  $G_N(k)$  has to be expected can be predicted in advance. But peaks at different values of  $k$  are also visible (thin gray lines); their positions depend on the discrete energy spectrum of the  $N$  detected neutrinos and thus both on input fluxes and on stochastic, finite statistics effects. When the Earth modulation effect is not sizable enough, its associated peak can be comparable to or shadowed by these features. In order to quantify the observability of the Earth effect peak, we compare the mean value of  $G_N(k)$  to the expected noise ( $\sim 1$ ). The fact that they are compatible at  $1\sigma$  means that the Earth effect will not produce a visible peak in at least the 68 % of cases. This situation is clearly visible in some of the plots of Fig. 4 (e.g. WC and SC at 1 kpc) in which the mean value of  $G_N(k)$  is always compatible with a null detection at  $1\sigma$ , despite the fact that some of the realizations exhibit a very well defined Earth effect peak.

Starting with a typical SN at  $d = 10$  kpc (left panels of Fig. 4),  $G_N(k) \simeq 1$  for  $k \gtrsim 40$ , for all the three detectors as expected in the absence of Earth modulation. No peak in  $G_N(k)$  associated with the Earth effect is visible. For a SN at  $d = 1$  kpc, a peak around  $k \simeq 70$  seems to emerge in the average  $G_N(k)$  for the WC and for the LS. However, the power spectrum is compatible with 1 at  $1\sigma$ , i.e. with the expectations without the Earth crossing. Conversely, in the case of LAr TPC the peak in  $G_N(k)$  is clearly visible at  $k \simeq 80$ . Indeed, this detector has the benefit of testing the Earth effect in the neutrino channel where the difference in the average energies/fluxes of  $\nu_e$  and  $\nu_x$  is larger than in the antineutrino sector. Therefore, the Earth signature is enhanced. We checked that the Earth effect starts to be visible in a LAr TPC at a few kpc for our benchmark SN neutrino fluxes. In the right panels of Fig. 4, we show the power spectrum for the lucky case of a very close-by SN at  $d = 0.2$  kpc. The peak in the power spectrum is clearly visible in the three different detectors. In particular, in the case of a liquid SC the superior energy resolution allows to see the double-peak structure in the power-spectrum discussed in Sec. 3.

We repeated the same analysis with other eight SN models from the Garching simulations with progenitor mass between 12 and  $40 M_\odot$  (see Fig. 1 in [6]) finding similar results to what shown before. Also for the accretion phase of the Basel/Darmstadt progenitors with  $10.8 M_\odot$  and  $18 M_\odot$  [17], our results are similar. Finally, we calculated the power-spectrum in presence of the Earth matter also during the cooling phase for the Basel/Darmstadt simulations, characterizing  $\nu$  oscillations as described in Sec. 3. We find that, since during this phase the spectral differences among different flavors are very small, no peak in the power spectrum appears even in the optimistic case of a very close-by SN (results not shown here).

As anticipated in the previous sections, the recent supernova simulations point towards mean energies that are lower than previously considered in the literature and and fluxes that are closer among themselves during the cooling phase.

As evident from Fig. 4, these spectral features generate a destructive interference in the power spectrum sometimes responsible for the appearance of a double peak and suppress the intensity of the expected Earth peak (see also Figs. 2,3). Moreover, we take into account the time-dependence of the neutrino fluxes and discuss a time-integrated analysis for both the accretion and the cooling phase. Therefore an eventual enhancement of the power spectrum peak due to a lucky choice of the spectral parameters (i.e., a choice of the initial fluxes corresponding to a particular post-bounce time, as in the existing literature) could be averaged out with the time integration. Of course, despite the major improvements on the simulations side over the last decade (e.g. on dimensionality, weak interaction physics, general relativity, etc.) one cannot exclude that the current supernova paradigm is oversimplified and forthcoming supernova simulations, including effects not yet considered (or new physics), might point towards an enhancement of the differences among the neutrino fluxes, allowing a better resolution for the Earth peak.

## B. Two detectors

The Earth effect could produce a modification in the SN  $\bar{\nu}_e$  light-curve measured by Icecube. Therefore, together with a high-statistics Mton WC detector it could detect the Earth effect (if only one of the two detectors is shadowed) by the relative difference in the temporal signals [16].

Figure 5 shows the ratio of the counting rate for IceCube and for a 400 kton WC detector, taking the input for the un-oscillated  $\nu$  fluxes from the accretion phase of the  $15 M_\odot$  Garching model. The counting rate in IceCube also includes the noise from the photomultipliers (280 Hz per optical module). We assume that the WC detector is un-shadowed. In the case that IceCube is shadowed we indicate the ratio of events with squares, while when Icecube is un-shadowed the ratio is plotted with circles. The left panel represents the ratio for a SN at 10 kpc, the central at 1 kpc, and the right at 0.2 kpc, respectively. In all the cases, we employ the time-dependent values of the parameters  $L_\nu$ ,  $\langle E_\nu \rangle$  and  $\alpha_\nu$  as obtained from  $15 M_\odot$  Garching model. Note also that the shape of the ratio changes with the distance of the SN, since the measured signal in Icecube is the sum of a time-independent background rate (independent of the distance) and a true SN lightcurve whose normalization depends on the distance.

The left panel clearly shows that the ratio with and without Earth matter effects are nearly inseparable for a SN at  $d = 10$  kpc, since the statistical errors are larger than the difference. For a SN at  $d = 1$  kpc, the ratio in the shadowed and un-shadowed case still have too large statistical errors to be clearly separated. Conversely, the shadowed and un-shadowed cases are statistically separable at  $d = 0.2$  kpc. However, since the differences between the two curves are relatively small (maximum difference  $\sim 1.7\%$  at 40 ms) and the the initial neutrino fluxes are not known with such precision, it is unlikely that the ratio of events could be used to diagnose the Earth effect, unless the comparison can be performed between two *very similar* detectors, with systematics canceling out. Otherwise, moderate variations in the distance of the SN events or the time-dependence used for the parameters ( $L_\nu$ ,  $\langle E_\nu \rangle$  and  $\alpha_\nu$ ) may alone alter the “reference” curve with respect to which compared an eventual signal.

## VI. CONCLUSIONS

The Earth matter effect in supernova neutrinos would be an interesting tool to diagnose the neutrino mass hierarchy at “large”  $\theta_{13}$ . Motivated by the recent measurement of this angle [41, 42] and by the vivid discussion for future large underground neutrino detectors, we found worthwhile to reevaluate the chance to detect this effect in future neutrino experiments. In order to achieve a realistic characterization of this signature, we adopted state-of-the-art SN simulation inputs [6, 17] to describe the un-oscillated SN neutrino signal. The detection of the modulation in the neutrino spectra induced by the Earth crossing largely depends on the neutrino average energies and on the flavor-dependent differences between the primary spectra. At this regard, recent supernova simulations indicate lower average energies than previously expected [6, 17, 18] and a tendency towards the equalization of the neutrino fluxes of different flavors during the cooling phase [19]. This makes the detection of the Earth matter effect more challenging than what assumed in previous works based on outdated SN simulations.

In order to diagnose the modulation in the SN  $\nu$  energy spectrum induced by the Earth crossing, we perform a Fourier analysis of the neutrino signal in a 400 kton WC detector, in a 50 kton liquid SC and in a 100 kton LAr TPC. For all these detectors, we found that coming from a typical galactic SN at  $d = 10$  kpc, no signature of the Earth matter effect is observable in the measured SN neutrino burst. Moreover, also in the more optimistic case of a close-by SN at  $d = 1$  kpc, the chances to detect the Earth matter signature appear statistically weak in the antineutrino signal. Conversely, a signal would show up in the  $\nu_e$  signal detectable at a LAr TPC. Only for relatively close stars which might evolve into core-collapse supernovae at unpredictable future times like Betelgeuse, Mira Ceti, and Antares (at  $d \lesssim 0.2$  kpc), the Earth matter signal would be detectable with high significance in both neutrino and antineutrino signals. Finally, Icecube taken as co-detector to monitor the Earth effect together with a Mton WC detector is not

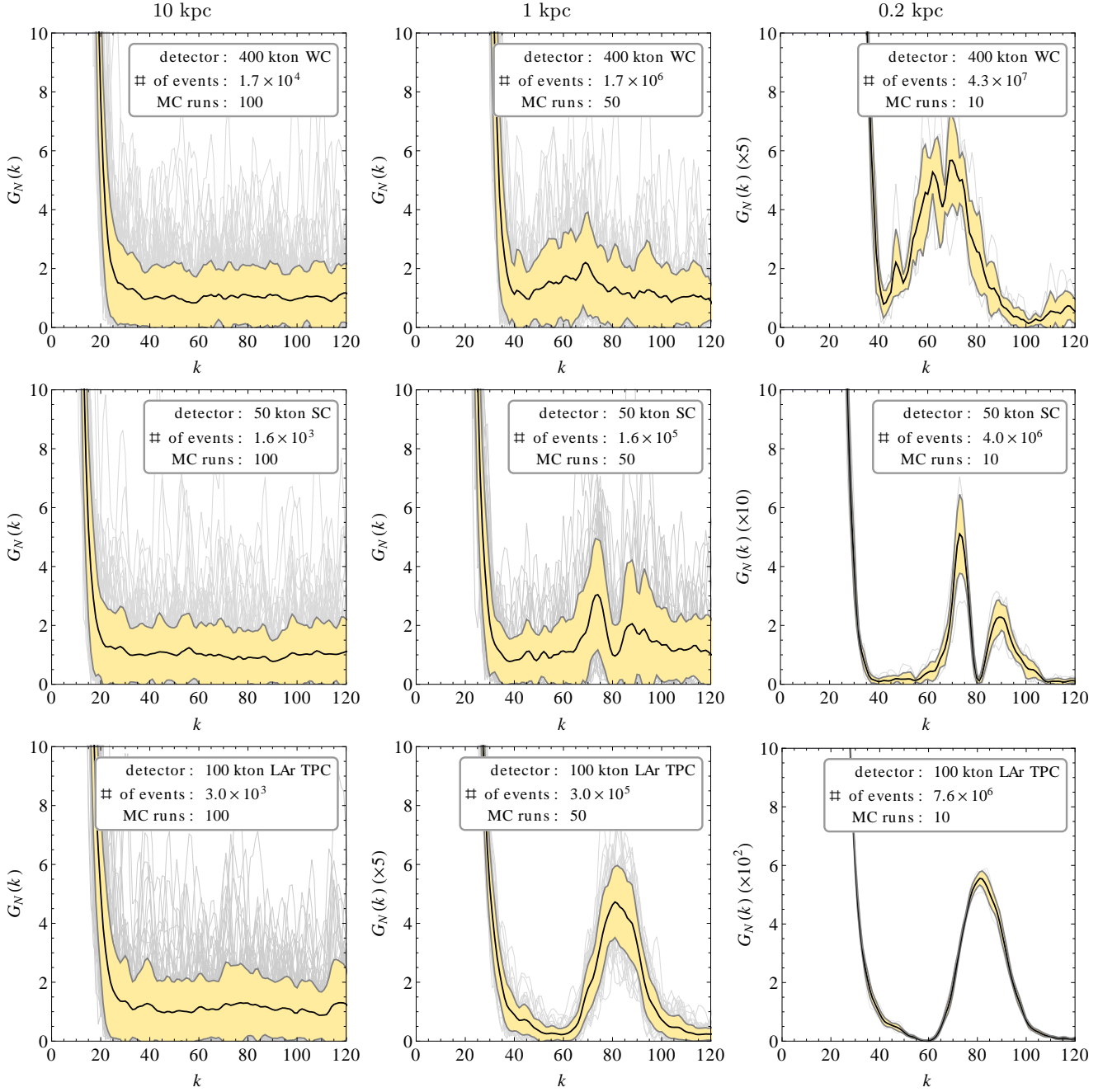


FIG. 4: Power spectrum  $G_N(k)$  of the Earth matter effect for a Galactic SN at  $d = 10$  kpc (left panels),  $d = 1$  kpc (central panels) and  $d = 0.2$  kpc (right panels). The upper panels refer to a 400 kton WC detector, the middle panels to a 50 kton SC, and the lower panels to a 100 kton LAr TPC. The light curves corresponds to different MonteCarlo realizations of the power spectrum  $G_N(k)$ , the thick curve to the average over the different realizations, and the band to the  $\pm 1\sigma$  variance level.

able to detect any sizeable variation in the SN neutrino event rate associated with the Earth matter effect for any galactic supernova.

These new results based on the state-of-art SN simulations dramatically change the previous perspectives of detection of the Earth matter effect with supernova neutrinos based on an outdated choice for the primary SN neutrino fluxes, as reported from previous supernova simulations. In particular, Mton WC detectors and large liquid scintillators would be able to observe the Earth matter signature only for very-close by (and rare) SNe, provided that the electronics of the detector will be able to cope with huge rates of events. A 100 kton LAr TPC which starts to monitor the Earth signature from SNe at a distance of few kpc from the Earth, would statistically have  $\sim 10\%$  of chance to

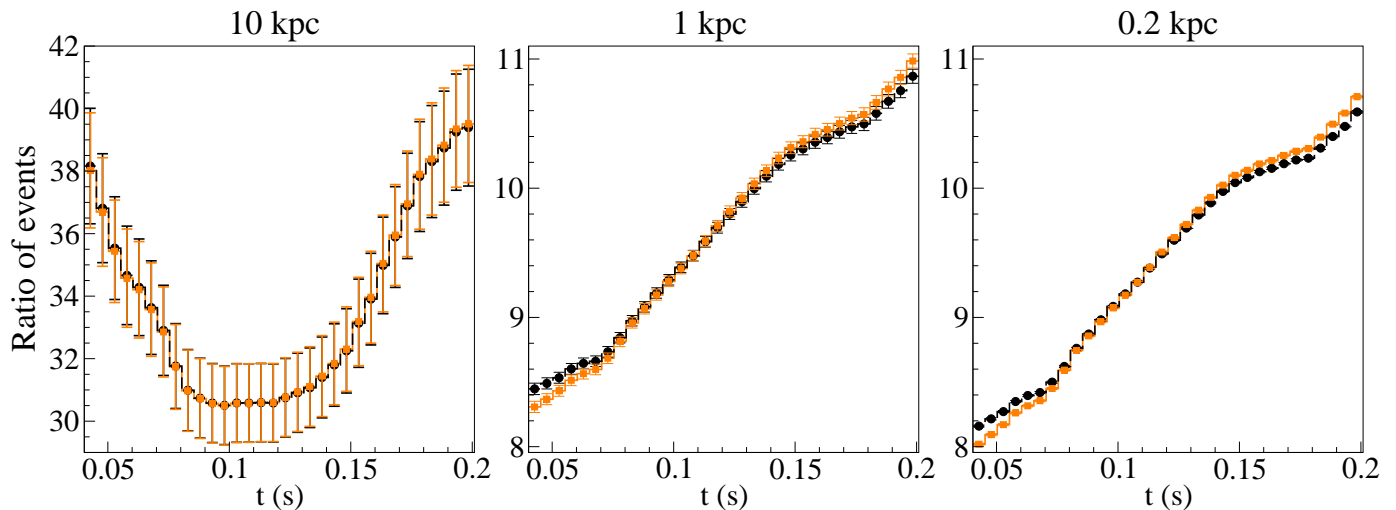


FIG. 5: Events ratio in IceCube with respect to a 400 kton WC detector. The Mton detector is always considered un-shadowed by the Earth. The case when IceCube is shadowed is shown with the orange squares, whereas the case of Icecube un-shadowed plotted by black circles. The left panel represents the events ratio for a SN at 10 kpc, the central at 1 kpc, and the right at 0.2 kpc, respectively.

see this signature from the next galactic supernova explosion [48].

As a consequence of our finding, the possibility to determine the neutrino mass hierarchy with the next galactic SN neutrino burst requires to be rediscussed. Of course, a caveat is that, while current SN simulations have improved in many ways with respect to one or two decades ago, the results obtained should still be considered as indicative, and an empirical test would certainly be welcome. Turning the argument around, we can say that—barring an exceptional situation of a close-by SN—a positive detection of the Earth matter effect in future data would come as a surprise and probably invalidate the current models. A negative result most likely would turn into constraints in the flavor flux difference vs. average energy differences parameter space, thus indirectly testing these models.

Of course, this should not discourage experimentalists to devote efforts to achieve a detailed measurement of the neutrino flux and spectra from a Galactic supernova; it would be “per se” a bonanza for testing the astrophysical models and the detailed understanding of the core-collapse SN mechanism.

If Earth matter effect in SNe is now not so promising as thought before, there are still other intriguing signatures in the SN neutrino signal that could give important information on the mass hierarchy. In particular, the early  $\nu_e$  neutronization peak that could be detected in a Mton WC detector or in a large LAr TPC would provide a clear signature to extract the neutrino mass hierarchy [5]. Also the early signal rise during the accretion phase, detectable by all the detectors discussed in this work, could encode an imprint of the neutrino mass ordering [6]. In conclusion, supernova neutrinos still represent a unique astrophysical probe of neutrino physics and astrophysics under extreme conditions.

### Acknowledgements

We are grateful to Tobias Fisher, Thomas Janka and collaborators for providing the supernova data. E.B. and I.T. thank Georg Raffelt for useful discussions. The work of E.B. was supported by LAGUNA-LBNO. The work of S.C. and A.M. was supported by the German Science Foundation (DFG) within the Collaborative Research Center 676 “Particles, Strings and the Early Universe”. I.T. acknowledges support from the Alexander von Humboldt Foundation, partial support from the Deutsche Forschungsgemeinschaft under grant EXC-153 and by the European Union FP7 ITN INVISIBLES (Marie Curie Actions, PITN-GA-2011-289442).

## References

- 
- [1] L. Wolfenstein, “Neutrino Oscillations In Matter,” *Phys. Rev. D* **17**, 2369 (1978); S. P. Mikheev and A. Yu. Smirnov, “Resonance Enhancement Of Oscillations In Matter And Solar Neutrino Spectroscopy,” *Yad. Fiz.* **42**, 1441 (1985) [*Sov. J. Nucl. Phys.* **42**, 913 (1985)].
- [2] A. S. Dighe and A. Yu. Smirnov, “Identifying the neutrino mass spectrum from the neutrino burst from a supernova,” *Phys. Rev. D* **62**, 033007 (2000) [hep-ph/9907423].
- [3] H. Duan, G. M. Fuller and Y. -Z. Qian, “Collective Neutrino Oscillations,” *Ann. Rev. Nucl. Part. Sci.* **60**, 569 (2010) [arXiv:1001.2799 [hep-ph]].
- [4] G. G. Raffelt, “Neutrinos and the stars,” arXiv:1201.1637 [astro-ph.SR].
- [5] M. Kachelriess, R. Tomàs, R. Buras, H. -T. Janka, A. Marek and M. Rampp, “Exploiting the neutronization burst of a galactic supernova,” *Phys. Rev. D* **71**, 063003 (2005) [astro-ph/0412082].
- [6] P. D. Serpico, S. Chakraborty, T. Fischer, L. Hudepohl, H. -T. Janka and A. Mirizzi, “Probing the neutrino mass hierarchy with the rise time of a supernova burst,” *Phys. Rev. D* **85**, 085031 (2012) [arXiv:1111.4483 [astro-ph.SR]].
- [7] R. C. Schirato, G. M. Fuller, “Connection between supernova shocks, flavor transformation, and the neutrino signal,” [astro-ph/0205390].
- [8] G. L. Fogli, E. Lisi, D. Montanino, A. Mirizzi, “Analysis of energy and time dependence of supernova shock effects on neutrino crossing probabilities,” *Phys. Rev. D* **68**, 033005 (2003) [hep-ph/0304056].
- [9] G. L. Fogli, E. Lisi, A. Mirizzi, D. Montanino, “Probing supernova shock waves and neutrino flavor transitions in next-generation water-Cherenkov detectors,” *JCAP* **0504**, 002 (2005) [hep-ph/0412046].
- [10] G. L. Fogli, E. Lisi, A. Mirizzi, D. Montanino, “Damping of supernova neutrino transitions in stochastic shock-wave density profiles,” *JCAP* **0606**, 012 (2006) [hep-ph/0603033].
- [11] R. Tomàs, M. Kachelriess, G. Raffelt, A. Dighe, H. -T. Janka, L. Scheck, “Neutrino signatures of supernova shock and reverse shock propagation,” *JCAP* **0409**, 015 (2004) [astro-ph/0407132].
- [12] C. Lunardini and A. Yu. Smirnov, “Supernova neutrinos: Earth matter effects and neutrino mass spectrum,” *Nucl. Phys. B* **616**, 307 (2001) [hep-ph/0106149].
- [13] B. Dasgupta, A. Dighe and A. Mirizzi, “Identifying neutrino mass hierarchy at extremely small  $\theta_{13}$  through Earth matter effects in a supernova signal,” *Phys. Rev. Lett.* **101**, 171801 (2008) [arXiv:0802.1481 [hep-ph]].
- [14] A. S. Dighe, M. T. Keil and G. G. Raffelt, “Identifying earth matter effects on supernova neutrinos at a single detector,” *JCAP* **0306**, 006 (2003) [hep-ph/0304150].
- [15] A. S. Dighe, M. Kachelriess, G. G. Raffelt and R. Tomàs, “Signatures of supernova neutrino oscillations in the earth mantle and core,” *JCAP* **0401**, 004 (2004) [hep-ph/0311172].
- [16] A. S. Dighe, M. T. Keil and G. G. Raffelt, “Detecting the neutrino mass hierarchy with a supernova at IceCube,” *JCAP* **0306**, 005 (2003) [hep-ph/0303210].
- [17] T. Fischer, S. C. Whitehouse, A. Mezzacappa, F. -K. Thielemann and M. Liebendörfer, “Proton-neutron star evolution and the neutrino driven wind in general relativistic neutrino radiation hydrodynamics simulations,” *Astron. Astrophys.* **517**, A80 (2010) [arXiv:0908.1871 [astro-ph.HE]].
- [18] L. Hudepohl, B. Müller, H. -T. Janka, A. Marek and G. G. Raffelt, “Neutrino Signal of Electron-Capture Supernovae from Core Collapse to Cooling,” *Phys. Rev. Lett.* **104**, 251101 (2010) [Erratum-ibid. **105**, 249901 (2010)] [arXiv:0912.0260 [astro-ph.SR]].
- [19] T. Fischer, G. Martínez-Pinedo, M. Hempel and M. Liebendörfer, “Neutrino spectra evolution during proto-neutron star deleptonization,” *Phys. Rev. D* **85**, 083003 (2012) [arXiv:1112.3842 [astro-ph.HE]].
- [20] B. Jegerlehner, F. Neubig and G. G. Raffelt, “Neutrino oscillations and the supernova SN1987A signal,” *Phys. Rev. D* **54**, 1194 (1996) [astro-ph/9601111].
- [21] A. Mirizzi and G. G. Raffelt, “New analysis of the sn 1987a neutrinos with a flexible spectral shape,” *Phys. Rev. D* **72**, 063001 (2005) [astro-ph/0508612].
- [22] A. de Bellefon *et al.*, “MEMPHYS: A Large scale water Cherenkov detector at Frejus,” hep-ex/0607026.
- [23] K. Abe *et al.*, “Letter of Intent: The Hyper-Kamiokande Experiment — Detector Design and Physics Potential —,” arXiv:1109.3262 [hep-ex].
- [24] M. Wurm *et al.* [LENA Collaboration], “The next-generation liquid-scintillator neutrino observatory LENA,” *Astropart. Phys.* **35**, 685 (2012) [arXiv:1104.5620 [astro-ph.IM]].
- [25] A. Badertscher *et al.*, “Giant Liquid Argon Observatory for Proton Decay, Neutrino Astrophysics and CP-violation in the Lepton Sector (GLACIER),” arXiv:1001.0076 [physics.ins-det].
- [26] D. Autiero *et al.*, “Large underground, liquid based detectors for astro-particle physics in Europe: Scientific case and prospects,” *JCAP* **0711**, 011 (2007) [arXiv:0705.0116 [hep-ph]].
- [27] T. Akiri *et al.* [LBNE Collaboration], “The 2010 Interim Report of the Long-Baseline Neutrino Experiment Collaboration Physics Working Groups,” arXiv:1110.6249 [hep-ex].
- [28] L. Kopke, “Supernova Neutrino Detection with IceCube,” *J. Phys. Conf. Ser.* **309**, 012029 (2011) [arXiv:1106.6225 [astro-ph.HE]].

- [29] M. T. Keil, G. G. Raffelt and H. -T. Janka, “Monte Carlo study of supernova neutrino spectra formation,” *Astrophys. J.* **590**, 971 (2003) [astro-ph/0208035].
- [30] G. G. Raffelt, “Mu- and tau-neutrino spectra formation in supernovae,” *Astrophys. J.* **561**, 890 (2001) [astro-ph/0105250].
- [31] G. L. Fogli, E. Lisi, A. Marrone, D. Montanino, A. Palazzo and A. M. Rotunno, “Global analysis of neutrino masses, mixings and phases: entering the era of leptonic CP violation searches,” *Phys. Rev. D* **86** (2012) 013012 [arXiv:1205.5254 [hep-ph]].
- [32] G. L. Fogli, E. Lisi, A. Marrone and A. Mirizzi, “Collective neutrino flavor transitions in supernovae and the role of trajectory averaging,” *JCAP* **0712**, 010 (2007) [arXiv:0707.1998 [hep-ph]].
- [33] G. L. Fogli, E. Lisi, A. Marrone, A. Mirizzi and I. Tamborra, “Low-energy spectral features of supernova (anti)neutrinos in inverted hierarchy,” *Phys. Rev. D* **78** (2008) 097301 [arXiv:0808.0807 [hep-ph]].
- [34] A. Mirizzi, R. Tomàs, “Multi-angle effects in self-induced oscillations for different supernova neutrino fluxes,” *Phys. Rev. D* **84**, 033013 (2011) [arXiv:1012.1339 [hep-ph]].
- [35] S. Chakraborty, T. Fischer, A. Mirizzi, N. Saviano, R. Tomàs, “No collective neutrino flavor conversions during the supernova accretion phase,” *Phys. Rev. Lett.* **107**, 151101 (2011) [arXiv:1104.4031 [hep-ph]].
- [36] S. Chakraborty, T. Fischer, A. Mirizzi, N. Saviano, R. Tomàs, “Analysis of matter suppression in collective neutrino oscillations during the supernova accretion phase,” *Phys. Rev. D* **84**, 025002 (2011) [arXiv:1105.1130 [hep-ph]].
- [37] N. Saviano, S. Chakraborty, T. Fischer and A. Mirizzi, “Stability analysis of collective neutrino oscillations in the supernova accretion phase with realistic energy and angle distributions,” *Phys. Rev. D* **85** (2012) 113002 [arXiv:1203.1484 [hep-ph]].
- [38] S. Sarikas, G. G. Raffelt, L. Hüdepohl and H. -T. Janka, “Suppression of Self-Induced Flavor Conversion in the Supernova Accretion Phase,” *Phys. Rev. Lett.* **108**, 061101 (2012) [arXiv:1109.3601 [astro-ph.SR]].
- [39] S. Sarikas, I. Tamborra, G. G. Raffelt, L. Hüdepohl and H. -T. Janka, “Supernova neutrino halo and the suppression of self-induced flavor conversion,” *Phys. Rev. D* **85** (2012) 113007 [arXiv:1204.0971 [hep-ph]].
- [40] A. Esteban-Pretel, A. Mirizzi, S. Pastor, R. Tomàs, G. G. Raffelt, P. D. Serpico, G. Sigl, “Role of dense matter in collective supernova neutrino transformations,” *Phys. Rev. D* **78**, 085012 (2008) [arXiv:0807.0659 [astro-ph]].
- [41] F. P. An *et al.* [DAYA-BAY Collaboration], “Observation of electron-antineutrino disappearance at Daya Bay,” *Phys. Rev. Lett.* **108**, 171803 (2012) [arXiv:1203.1669 [hep-ex]].
- [42] J. K. Ahn *et al.* [RENO Collaboration], “Observation of Reactor Electron Antineutrino Disappearance in the RENO Experiment,” arXiv:1204.0626 [hep-ex].
- [43] B. Dasgupta, A. Dighe, G. G. Raffelt and A. Yu. Smirnov, “Multiple Spectral Splits of Supernova Neutrinos,” *Phys. Rev. Lett.* **103** (2009) 051105 [arXiv:0904.3542 [hep-ph]].
- [44] G. Fogli, E. Lisi, A. Marrone and I. Tamborra, “Supernova neutrinos and antineutrinos: Ternary luminosity diagram and spectral split patterns,” *JCAP* **0910** (2009) 002 [arXiv:0907.5115 [hep-ph]].
- [45] C. Lunardini and I. Tamborra, “Diffuse supernova neutrinos: oscillation effects, stellar cooling and progenitor mass dependence,” *JCAP* **07**, 012 (2012) [arXiv:1205.6292 [astro-ph.SR]].
- [46] A. Friedland and A. Gruzinov, “Neutrino signatures of supernova turbulence,” astro-ph/0607244.
- [47] J. P. Kneller and C. Volpe, “Turbulence effects on supernova neutrinos,” *Phys. Rev. D* **82**, 123004 (2010) [arXiv:1006.0913 [hep-ph]].
- [48] A. Mirizzi, G. G. Raffelt and P. D. Serpico, “Earth matter effects in supernova neutrinos: Optimal detector locations,” *JCAP* **0605**, 012 (2006) [astro-ph/0604300].
- [49] G. L. Fogli, E. Lisi, D. Montanino and A. Palazzo, “Supernova neutrino oscillations: A Simple analytical approach,” *Phys. Rev. D* **65**, 073008 (2002) [Erratum-ibid. *D* **66**, 039901 (2002)] [hep-ph/0111199].
- [50] G. G. Raffelt, M. T. Keil, R. Buras, H. -T. Janka and M. Rampp, “Supernova neutrinos: Flavor-dependent fluxes and spectra,” astro-ph/0303226.
- [51] G. L. Fogli, E. Lisi, A. Mirizzi and D. Montanino, “Probing supernova shock waves and neutrino flavor transitions in next-generation water-Cherenkov detectors,” *JCAP* **0504**, 002 (2005) [hep-ph/0412046].
- [52] A. Strumia and F. Vissani, “Precise quasielastic neutrino/nucleon cross-section,” *Phys. Lett. B* **564**, 42 (2003) [astro-ph/0302055].
- [53] M. Wurm *et al.*, “Detection potential for the diffuse supernova neutrino background in the large liquid-scintillator detector LENA,” *Phys. Rev. D* **75**, 023007 (2007) [astro-ph/0701305].
- [54] A. G. Cocco, A. Ereditato, G. Fiorillo, G. Mangano and V. Pettorino, “Supernova relic neutrinos in liquid argon detectors,” *JCAP* **0412**, 002 (2004) [hep-ph/0408031].
- [55] I. Gil Botella and A. Rubbia, “Oscillation effects on supernova neutrino rates and spectra and detection of the shock breakout in a liquid argon TPC,” *JCAP* **0310**, 009 (2003) [hep-ph/0307244].
- [56] I. Gil Botella and A. Rubbia, “Decoupling supernova and neutrino oscillation physics with LAr TPC detectors,” *JCAP* **0408**, 001 (2004) [hep-ph/0404151].
- [57] R. Abbasi *et al.* [IceCube Collaboration], “IceCube Sensitivity for Low-Energy Neutrinos from Nearby Supernovae,” arXiv:1108.0171 [astro-ph.HE].